International Journal of Biotechnology Research ISSN: 0974-6293
Vol.11 No.1 january-June 2018

Modeling in the Development of an Elasto-Optical Biosensor Based on Nanostructures

N. D. Botkin[1], K.-H. Hoffmann[1], D. Marx[2], V. N. Starovoitov[3], and V. L. Turova[1]

Abstract: This paper presents numerical simulations related to the development of an elasto-optical biosensor (ELOBIS) consisting of a single polymer molecule and based on the Fluorescence Resonant Energy Transfer (FRET) effect. It is demonstrated that numerical simulations have provided important hints on the implementation of ELOBIS.

1. Introduction

The field of bioanalytics has evolved rapidly in recent years, focusing on the development of reliable methods for the detection of biomolecules such as DNA, RNA, proteins, antibodies, reaction products from human body functions, etc. In this paper, we discuss simulations that have been done to support the development of a new optical method for the detection of biosubstances (see [1]).

The principle proposed in [1] is based on the Fluorescence Resonant Energy Transfer (FRET), see [2, 3], within a capture molecule attached onto a nanostructured surface or nanoparticle. By applying a global excitation using either periodic or aperiodic mechanical, electrical, or magnetic forces, the distance between the two fluorophoric centers within the elastic detection molecule changes (becomes larger than the Förster radius, R_F), and thus the individual emittance of the two optical active centers will vary due to the changed FRET. The counter force against the excitation, entropy elasticity, will drive the polymer chain back to a mean reference elongation state. However, if the detection molecule bonds to an analyte molecule (see Fig. 1),

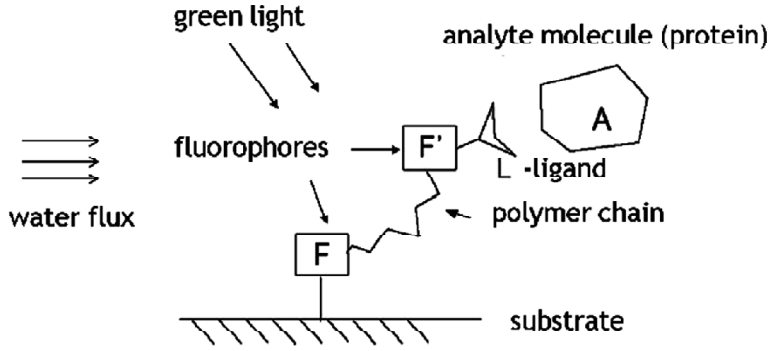

Figure 1: Sketch of the Detection Principle. If the Chain is Free, The Distance Between Fluorophores is Less Than the Förster Radius R_F, and Red Photons are Being Reemitted. If the Analyte Molecule is Trapped, The Polymer Chain Being Elongated so that the Distance Between the Fluorophores Becomes Larger than R_F, and Green Photons are Being Reemitted.

[1] Technische Universitäat Munchen, Mathematics Centre.

[2] Humboldt University of Berlin.

[3] Lavrentyev's Institute of Hydrodynamics of Siberian Branch of RAS.

the elongation will change and thus the corresponding change in optical response will give a fingerprint of the trapping. The measurement of spectral changes can be done by an optical confocal microscope with optical detectors.

The main problem consists in the implementation of a proper mechanical excitation of the elastic detection molecule to provide its elongation in the case of binding of the analyte molecule. Different excitation principles have been analyzed, and the majority of them are not suitable for the application. Limitations are stipulated by nanometer size effects in fluids. Atomistically, near a surface, fluid molecules behave very different, establishing a decreased mobility zone decaying with 1/distance from the surface. Therefore, an elastic polymer immobilized on a substrate can only be stretched by large shear forces within the fluid. Mechanical ultrasound vibration, for example, does not provide large enough shear amplitudes. Static and dynamic electrical fields are shielded by the polarization of the water solvent. Electro-osmosis does also not provide large enough shear velocities.

The paper outlines such attempts and presents simulations that have provided a good hint on the right solution of this problem.

2. Polymer Chains in Good Solvents

This section discusses properties of polymer chains in good solvents where chains swell in order to maximize the number of polymer-fluid contacts. Chains oscillate due to the Brownian motion and assume all admissible configurations.

The results of the monograph [4] are used here.

2.1 Ideal (or Freely-Jointed) Chains

For ideal chains, fixed length polymer segments are linearly connected, and all bond and torsion angles are equiprobable. Let $\vec{R}_i$, $i = 1, ..., N$ be the vector connecting monomers $i - 1$ and i, and $\vec{R} = \sum_{i=1}^{N} \vec{R}_i$ the end-to-end vector. The mean square end-to-end distance, R^*, is computed as follows:

$$R^* := \langle \vec{R}^2 \rangle^{\frac{1}{2}} = lN^{1/2},$$

where the angle brackets denote mean value of a random variable, and l is the length of polymer segments.

The relative fluctuation, θ, of the quadratic end-to-end distance is given by

$$\theta = \frac{\langle (\vec{R}^2 - \langle \vec{R}^2 \rangle)^2 \rangle}{\langle \vec{R}^2 \rangle^2} = 2/3,$$

which means that there is no clear-cut “mean” conformation of the coil.

Another interesting characteristic of a Gaussian coil is its density, n, defined as the ratio of the total volume of balls of radius l covering the chain to the volume of a ball of radius R^*:

$$n = Nl^3/(lN^{1/2})^3 \sim N^{-1/2}.$$

The last formula points out to loosely packing of the coil structure. Nevertheless, a Gaussian coil in a moving fluid is subjected to the Stokes drag force, F_S, given by

$$F_S = 6\pi\nu v R_D, \tag{1}$$

where ν is the viscosity, v the fluid velocity, and R_D the hydrodynamical radius defined as

$$R_D = \left(\frac{1}{2} N^{-2} \left\langle \sum_{i=1}^{N} \sum_{j=1(j\neq i)}^{N} \left| \vec{R}_i - \vec{R}_j \right|^{-1} \right\rangle \right)^{-1} \approx 0.54 R^* . \tag{2}$$

It should be noticed that the estimation of the Stokes drag force could be larger, if micropolar properties of the moving fluid would be accounted for (see [12]).

Finally, the elasticity of a polymer chain is given by

$$\left| \langle \vec{R} \rangle \right| = lN \frac{l \left| \vec{F}_{el} \right|}{3k_B T},$$

where $\vec{F}_{el}$ is the stretching force, k_B the Boltzmann constant, and T the temperature.

2.2 Chains with the Excluded Volume

The excluded volume causes a reduction in the conformational possibilities of the chain and leads to a self-avoiding random walk. The expressions for the mean square end-to-end distance, R^*, is now given by

$$R^* = aN^{3/5}, \tag{3}$$

where a is the so called effective segment length which is a few larger than the geometrical length, l, of the segment. For example, some computations yield $a = 0.57$ in the case where $l = 0.5$.

The elasticity is described by the formula

$$\left| \langle \vec{R} \rangle \right| = aN \left(\frac{a \left| \vec{F}_{el} \right|}{3k_B T} \right)^{2/3}, \tag{4}$$

which allows us to estimate the necessary velocity, v, of the ambient fluid to reach the elongation R_F of the chain. Taking into account formulae (1), (2), (3), and (4) yields the equation

$$aN \left(\frac{a \left| 6\pi\nu v\, 0.54 R^* \right|}{3k_B T} \right)^{2/3} = R_F = 5\,nm .$$

Taking $N = 30$ and $a = 0.57$ nm yields the value $v \approx 0.3$ m/s.

The next section presents molecular dynamics simulations that confirm our estimation of the elongation of a polymer chain with the excluded volume in a moving fluid. On the other hand, these simulations show that the necessary elongation occurs in a quiescent fluid, if the detection molecule bonds to a great analyte molecule.

3. DISSIPATIVE PARTICLE DYNAMICS SIMULATIONS

Dissipative particle dynamics (DPD), see [5]-[10], is characterized by coarse graining in particle representation and a simplified description of interparticle interactions, which allows studies of systems at mesoscopic length and time scales. Particles represent whole molecules or fluid regions, rather than single atoms, and atomistic details are not considered relevant to the processes addressed. The particles internal degrees of freedom are integrated out and replaced by simplified pairwise dissipative and random forces,

so as to conserve momentum locally and ensure correct hydrodynamic behavior. The main advantage of this method is that it gives access to longer time and length scales than it would be possible using conventional molecular dynamic (MD) simulations. Notice that single beads can be connected into chains by tying them together with soft (often Hookean) springs so that polymer chains interacting with fluid molecules can be included in DPD models.

We study a system described by N_p particles (see [11]). The mass of particle i is denoted by m_i, and its position and velocity by $\vec{r}_i$ and $\vec{v}_i$, respectively. Interparticle interactions are characterized by the pairwise conservative, dissipative, and random forces exerted on particle i by particle j, respectively, and are given by

$$F_{ij}^C = a_{ij}\,\omega^C(r_{ij})\,\vec{e}_{ij}, \qquad F_{ij}^D = -\gamma\omega^D(r_{ij})(\vec{v}_{ij},\vec{e}_{ij})\vec{e}_{ij}, \qquad F_{ij}^R = \sigma\xi_{ij}\,\omega^R(r_{ij})\,\vec{e}_{ij},$$

where $\vec{r}_{ij} = \vec{r}_i - \vec{r}_j$, $\vec{v}_{ij} = \vec{v}_i - \vec{v}_j$, $r_{ij} = |\vec{r}_{ij}|$, $\vec{e}_{ij} = \vec{r}_{ij}/r_{ij}$, a_{ij} the amplitude of conservative forces, γ a dissipation constant defining viscosity, σ an excitation constant defining the temperature, and ξ_{ij} the Gaussian random variable. The pairwise conservative force is written in terms of the weight function $\omega^C(r)$ which is chosen e.g. as

$$\omega^C(r) = -\frac{\partial}{\partial r}U_{LJ}(r),$$

where $U_{LJ}(r) = 4\epsilon[(\delta/r)^{12} - (\delta/r)^6]$ is the Lenard-Jones potential. Here ϵ is the depth of the potential well, δ is the finite distance at which the interparticle potential is zero, and r is the distance between the particles. To account for the polymer chain, the weight function $\omega^C(r)$ is complemented by a harmonic potential between adjacent beads. Thus, the energy of the chain is

$$U_{\text{chain}} = -\frac{1}{2}k\sum_{i=1}^{N-1} r_{i,i+1}^2.$$

The strength of the conservative force a_{ij} has three different values depending on the pair of particles (water-water, water-monomer, monomer-monomer).

The weight function $\omega^R(r)$ is usually defined as

$$\omega^R(r) = \begin{cases} 1 - r/r_c, & r \le r_c, \\ 0, & r > r_c, \end{cases}$$

where r_c is a cut-off distance. The weight functions $\omega^D(r)$ and $\omega^R(r)$ of the dissipative and random forces are coupled since the thermal heat generated by the random force must be balanced by dissipation. The precise relationship between these two forces is determined by the fluctuation dissipation theorem (see e.g. [8]), and can be expressed as follows:

$$\omega^D(r) = [\omega^R(r)]^2, \qquad \sigma = 2\gamma k_B T^*,$$

where T^* is the temperature of the system.

The forces exerted on particle i are computed as follows:

$$\vec{F}_i^C = \sum_{j\neq i}\vec{F}_{ij}^C, \qquad \vec{F}_i^D = \sum_{j\neq i}\vec{F}_{ij}^D, \qquad \vec{F}_i^R = \sum_{j\neq i}\vec{F}_{ij}^R,$$

and the equations of motions are given as

$$d\vec{r}_i = \vec{v}_i\,dt,$$
$$d\vec{v}_i = \frac{1}{m_i}\left(\vec{F}_i^{\,C}dt + \vec{F}_i^{\,D}dt + \vec{F}_i^{\,R}\sqrt{dt}\right) \tag{5}$$

Assuming that a_{ij} = 3, 10, 10 for the monomer-water, monomer-monomer, and water-water interaction, respectively, and letting r_c = 1 nm, T^* = 300 K, $k_B = 1.38 \cdot 10^{-23}$ J/K, $m_i \approx 3 \cdot 10^{-26}$ kg, we obtain the following time unit and molecular velocity scale: $\tau \approx 2.6 \cdot 10^{-3}$ ns, $v_i \approx 370$ m/s.

Figure 2 sketches interactions between molecules, fixation of the polymer chain, and fold-back and reflection rules.

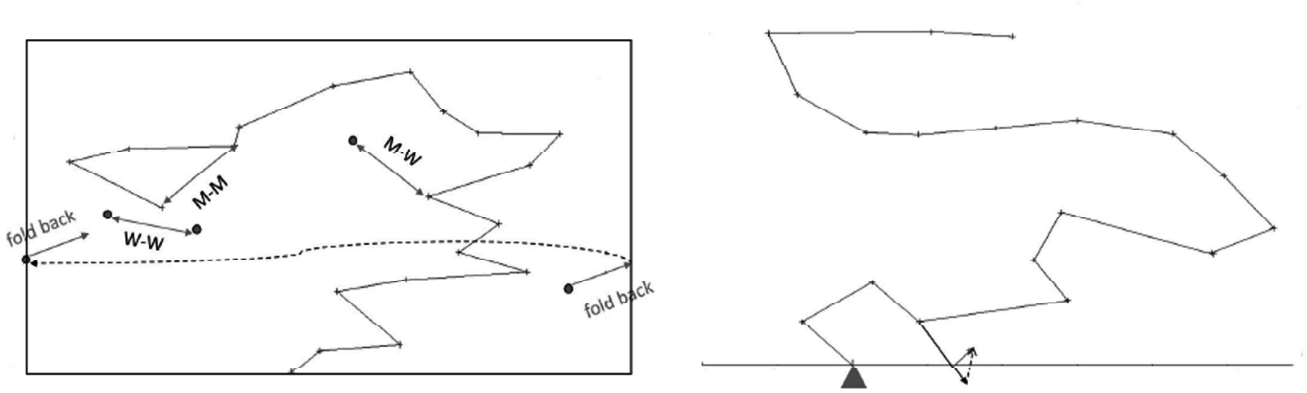

Figure 2: A sketch of Interactions Between Molecules and a Fold-Back Rule are Shown (to the Left). Here, "*W*" Denotes Water Molecules, and "*M*" Stands for Monomers of the Polymer Chain. Fixation of the Polymer Chain (to the Right) is Achieved Using a Very Strong Attractive Force Between the First Monomer Molecule of the Polymer Chain and a Point of the Substrate. The Reflection Rule for Water and Monomer Molecules is Sketched (to the Right).

During the simulation, the following problem has arisen. Water molecules under consideration are contained in a box with the edge of 30 nm. To simulate the flow, an initial velocity is prescribed for all water molecules. Obviously, there should be a very fast decay of this velocity (see Figure 3, to the left) because of the momentum transfer from water molecules to the polymer chain and finally to the substrate. To stabilize the velocity of the center of mass of water molecules, an additional force was applied to each water molecule. In other words, a feedback controller was added to each equation describing water molecules as follows:

$$m_i d\vec{v}_i = \vec{F}_i^{\,C}dt + \vec{F}_i^{\,D}dt + \vec{F}_i^{\,R}\sqrt{dt} - \lambda(\vec{v}_c - \vec{v}_0)\,dt, \qquad i \in W\,.$$

Here W is the set of integers indexing water molecules, $\vec{v}_0$ the desired velocity of the center of mass of water molecules, and $\vec{v}_c$ the baricentric velocity defined as

$$\vec{v}_c = \frac{1}{|W|}\sum_{i \in W}\vec{v}_i\,.$$

It is easily to prove (see [11]) that the following stabilization can be achieved:

$$|\vec{v}_c - \vec{v}_0| \sim \frac{\epsilon}{|W|} + \exp\left(-\frac{\lambda}{m}t\right),$$

where ϵ is the rate of the momentum transfer to the polymer chain, and m is the mass of water molecule. In simulations, parameter λ was chosen from the interval $10 \div 50$. Figure 3 (to the right) shows a very good stabilization of $\vec{v}_c$.

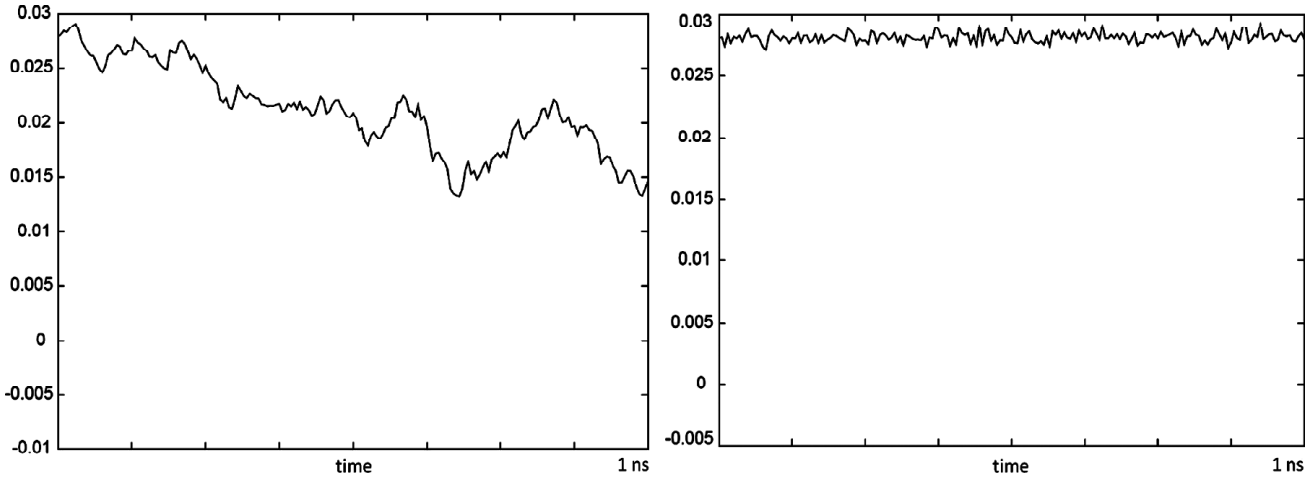

Figure 3: Decay of the Velocity of the Center of Mass of Water Molecules (to the Left) and the Result of a Stabilizing Feedback Procedure (to the Right)

Accounting for the analyte molecule (see Fig. 1) was implemented in several ways.

1. The analyte molecule is modeled as a ball strongly reflecting all impacting water molecules.
2. The analyte molecule is modeled through a repulsive potential that reflects impacting water molecules.
3. The analyte molecule is modeled by a chain consisting of monomers that strongly attract to each other and form a coil.

All these methods yield almost the same results. Nevertheless, the second one is more preferable because of its simpler implementation.

Simulations were performed using a free FORTRAN 90 software proposed by [13] and adopted to our aims as described above. A water box with the edge of 30 nm was considered, and the number of water molecules was appropriately chosen to provide the standard water density. The time scale varied from 1 to 100 ns.

Figure 4 shows simulation results. Curve (a) shows the elongation of the chain (nm) versus the flow velocity (m/s) in the case of captured analyte molecule. This result is very close to a theoretical estimation obtained on the base of work [14]. Curve (b) presents the result in the case of free chain (without binding of the analyte molecule).

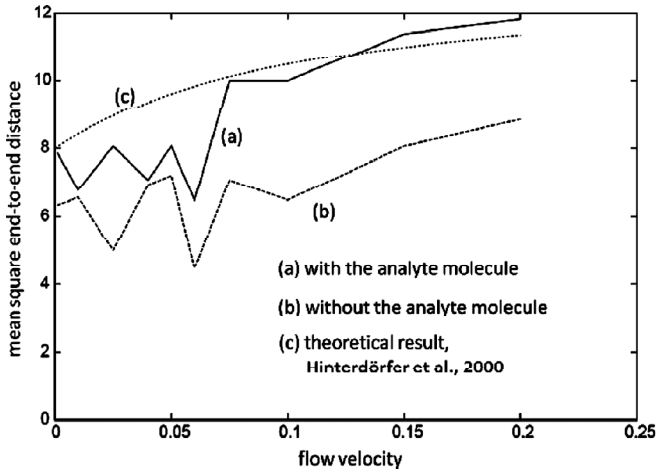

Figure 4: Simulation Results and Theoretical Prediction Based on the Estimation of the Elasticity of the Chain and the Stokes Drag Force

It can be easily seen that the necessary magnitude of velocity is not too large. The difficulty is that the polymer chain lies in a boundary layer where the flow velocity is close to zero. The thickness of such a layer approximately equals 200 – 300 nm. Thus, the idea to put the polymer chain to the top of a nanocone with 300 nm height has been examined. Figure 5 shows an array of nanocones (to the left) and the velocity magnitude (in percent to the incoming flow velocity) versus the vertical distance from the top of nanocones marked as 1 and 2 (to the right).

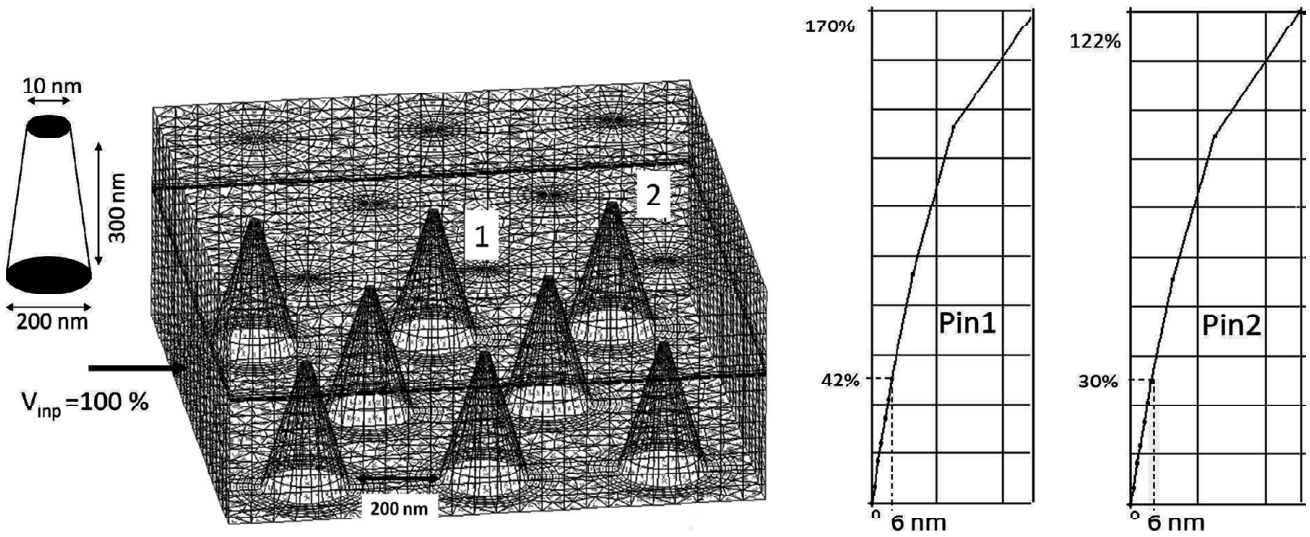

Figure 5: An Array of Nanocones (to the Left). Profiles of the Flow Velocity versus the Distance from the Top of Nanocones (to the Right)

The difficult arising here is related to the fabrication of an appropriate nanocone array and to the immobilization of polymer chains on tops of nanocones. Some experiments on the fabrication of nanocones have been performed by Prof. M. Giersig und Dr. M. Hilgendorff (see Figure 6).

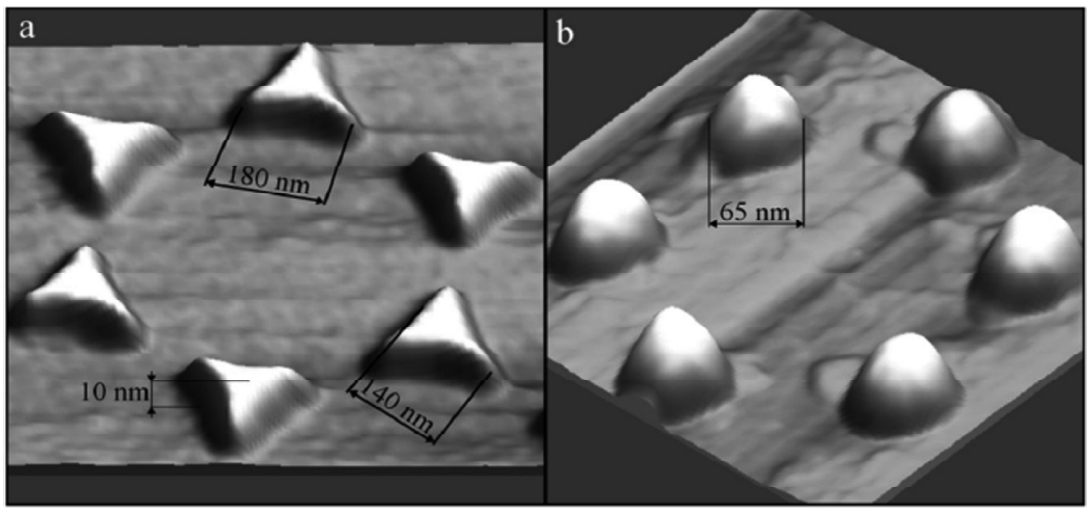

Figure 6: Nanoislands Prepared by Prof. M. Giersig und Dr. M. Hilgendorff to Prove the Idea of Nanocones

It should be noticed that the height of the islands is not sufficient because higher and thinner islands show instabilities. Moreover, the exact immobilization of the ELOBIS structure at the top of an island is very difficult. Therefore, the idea of the elongation of the ELOBIS structure using a global flow of the ambient fluid fails.

4. Simulation of Non Fixed Polymer Chains in Immovable Liquids

This section presents the idea to consider non fixed polymer chains in immovable fluids. The elongation of the polymer chain is expected due to the restriction on the number of possible conformations in the case of binding of a great analyte molecule. DPD simulations substantiate this idea and justify requirements on characteristics of the ELOBIS system.

Figure 7 shows two time series for the Gaussian random process, square of the end-to-end vector, $|\vec{R}|^2$. The solid line corresponds to the case of binding of a great analyte molecule. The mean square end-to-end distance equals 6.17 nm. The dotted line corresponds to the case of free polymer chain. The mean square end-to-end distance equals 5.47 nm in this case.

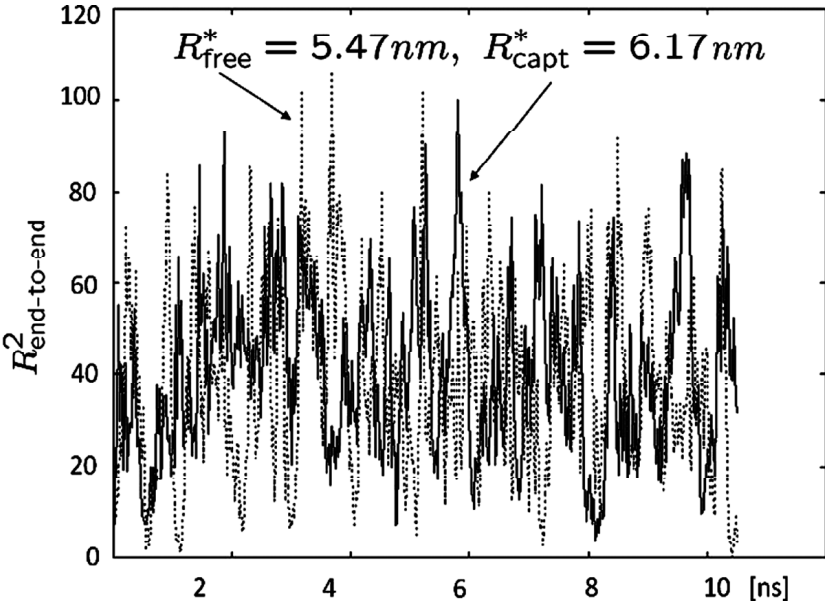

Figure 7: Time Series for the Gaussian Random Process $|\vec{R}|^2$. The Solid Line Corresponds to the Case of Binding of the Analyte Molecule. The Dotted line Describes the Case of Free Polymer Chain

Figure 8 shows the probability density functions for the random variable $|\vec{R}|$.

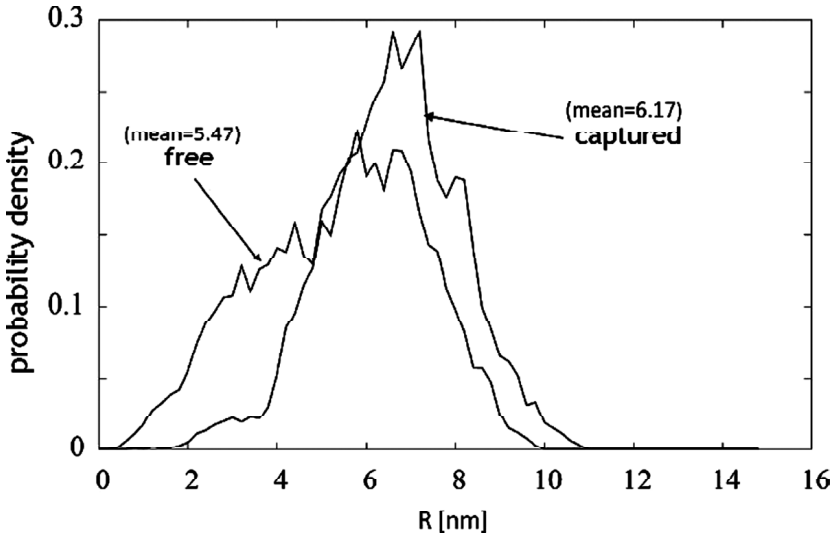

Figure 8: Probability Density Functions for the Random Variable $|\vec{R}|$. The Cases of Binding and Non-Binding of the Aanalyte Molecule are Shown

Figure 9 shows the probability (cumulative) distribution functions of $|\vec{R}|$. The distributions corresponding to the cases of binding and non-biding of the analyte molecule are easily distinguishable.

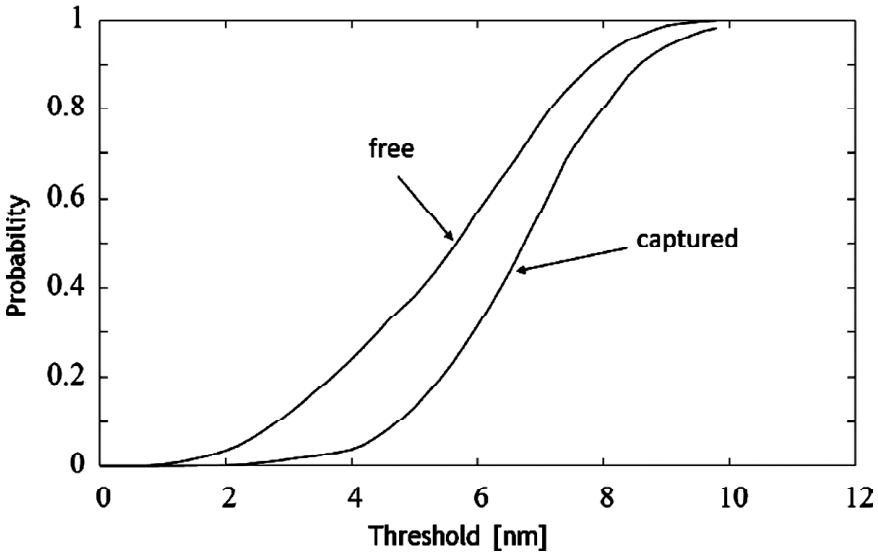

Figure 9: Probability (Cumulative) Distribution Functions for the Random Variable $|\vec{R}|$. The Cases of Binding and Non-Binding of the Analyte Molecule are Shown

Figure 10 shows the probability (cumulative) distribution functions of $|\vec{R}|$ in the case of a rough time sampling (0.1 ns). It is seen that a large sampling step disturbs the result not too much.

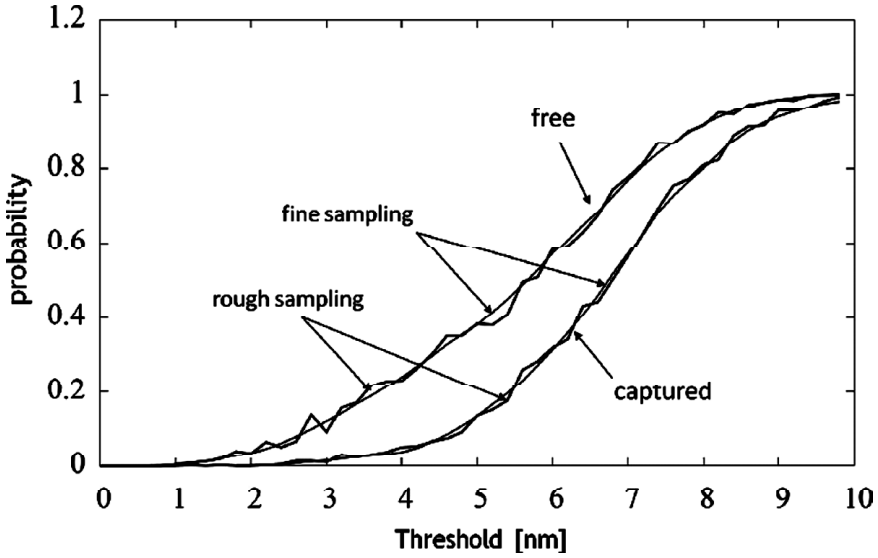

Figure 10: Probability (Cumulative) Distribution Functions for the Random Variable $|\vec{R}|$ in the Case of a Rough Time Sampling (0.1 ns)

Figure 11 shows a sketch of experimental setting. A green light source emits green photons that are adsorbed by the donor fluorophore and reemitted by the acceptor one. Depending on the distance between the flurophores, green or red photons are being produced. A confocal microscope which can separately register green and red photons measures the intensities of green and red light. Notice that the sensitivity of such a plant is approximately 50 photons so that our simulations should be averaged over 50 oscillations.

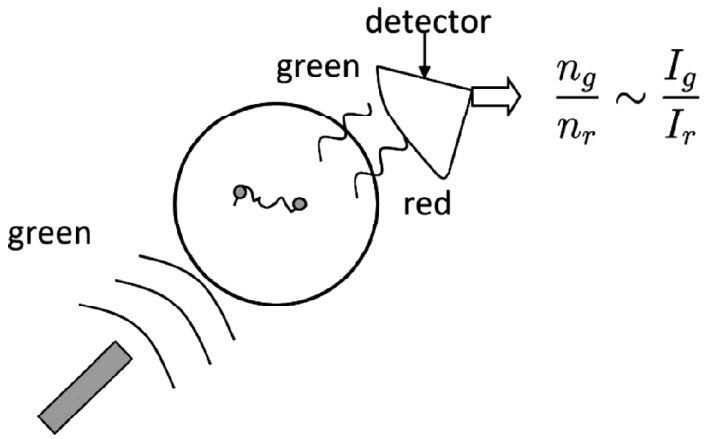

Figure 11: A Sketch of Experimental Setting. The Ratio, n_g/n_r, of the Numbers of Green and Red Photons is Proportional to the Ratio, I_g/I_r, of the Intensities of Green and Red Light. The Sensitivity Approximately Equals 50 Photons

Figure 12 shows a time series for $|\vec{R}|$ averaged over each 50 oscillations.

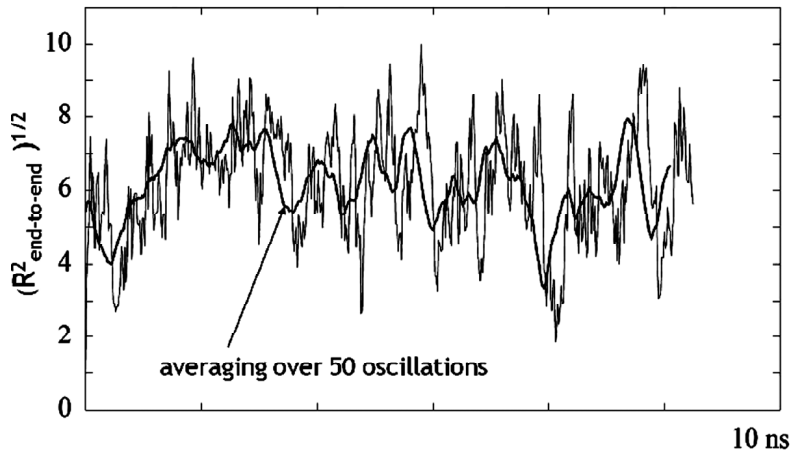

Figure 12: Averaging of a Time Series for $|\vec{R}|$ Over Each 50 Oscillations

Figure 13 shows the probability density functions for $|\vec{R}|$ in the case of averaging over each 50 oscillations. As it is expected, the pics of the distributions become sharper. They are clearly distinguishable.

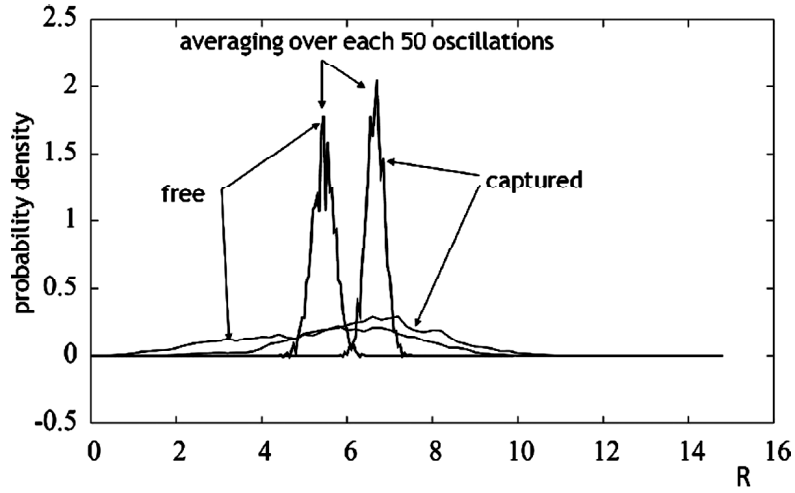

Figure 13: The Probability Density Functions for $|\vec{R}|$ in the Case of Averaging Over Each 50 oscillations

Figure 14 shows the probability (cumulative) distribution functions for $|\vec{R}|$ in the case of averaging over each 50 oscillations. The distributions are clearly distinguishable.

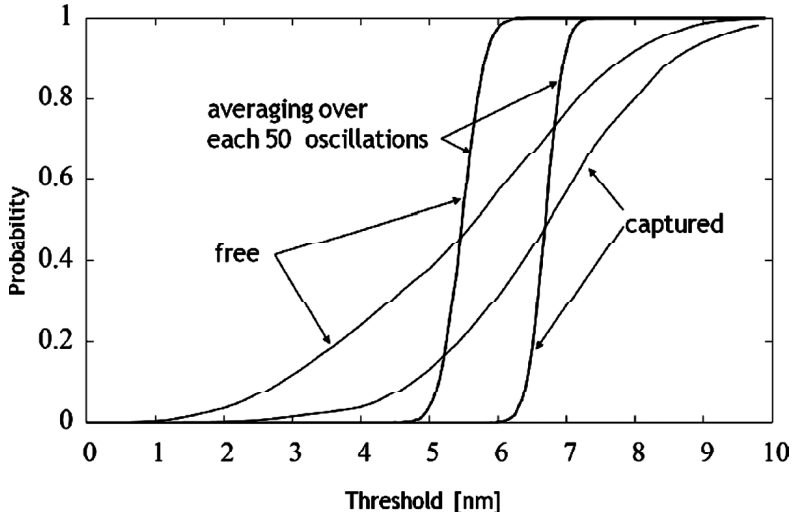

Figure 14: The Probability (Cumulative) Distribution Functions for $|\vec{R}|$ in the Case of Averaging Over Each 50 Oscillations

The simulations presented in this section substantiate the assumption that a freely drifting in an immovable fluid polymer chain exhibits an essential elongation without any mechanical excitation in the case of binding of a large analyte molecule. Therefore, the ELOBIS system does not need any artificial mechanisms exerting forces on the bound analyte molecule.

5. EXPERIMENTS

An ELOBIS structure (see Figure 15) has been constructed by the working group of Prof. Claus Seidel at the University of Düsseldorf. The system is not immobilized on a substrate but immersed in a solvent containing analyte molecules (avidin). A confocal microscope that can separately register green and red photons has been involved into the experiment. Two photo detectors have measured the intensities of green and red light. The measured distribution of S_G/S_R, the ratio of the intensities of green and red light, is shown in Figure 16. It is seen that the S_G/S_R is larger in the case where the ELOBIS system is bound with avidin. In other words, the detection of avidin occurs, which proves the idea of the sensor.

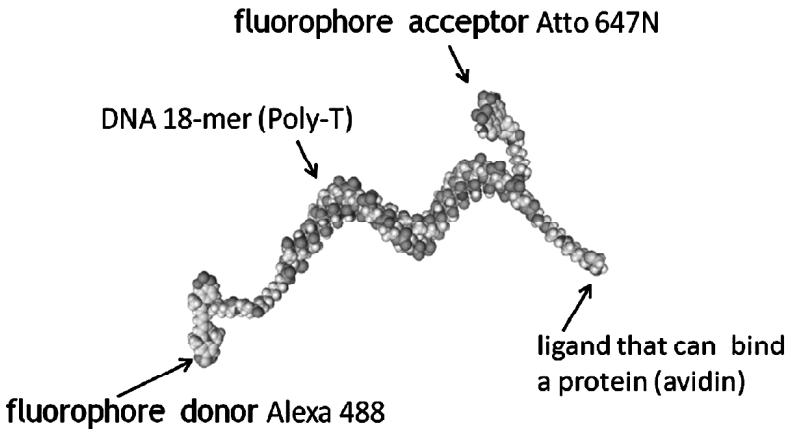

Figure 15: An ELOBIOS System Created by the Working Group of Prof. Claus Seidel at the University of Düsseldorf

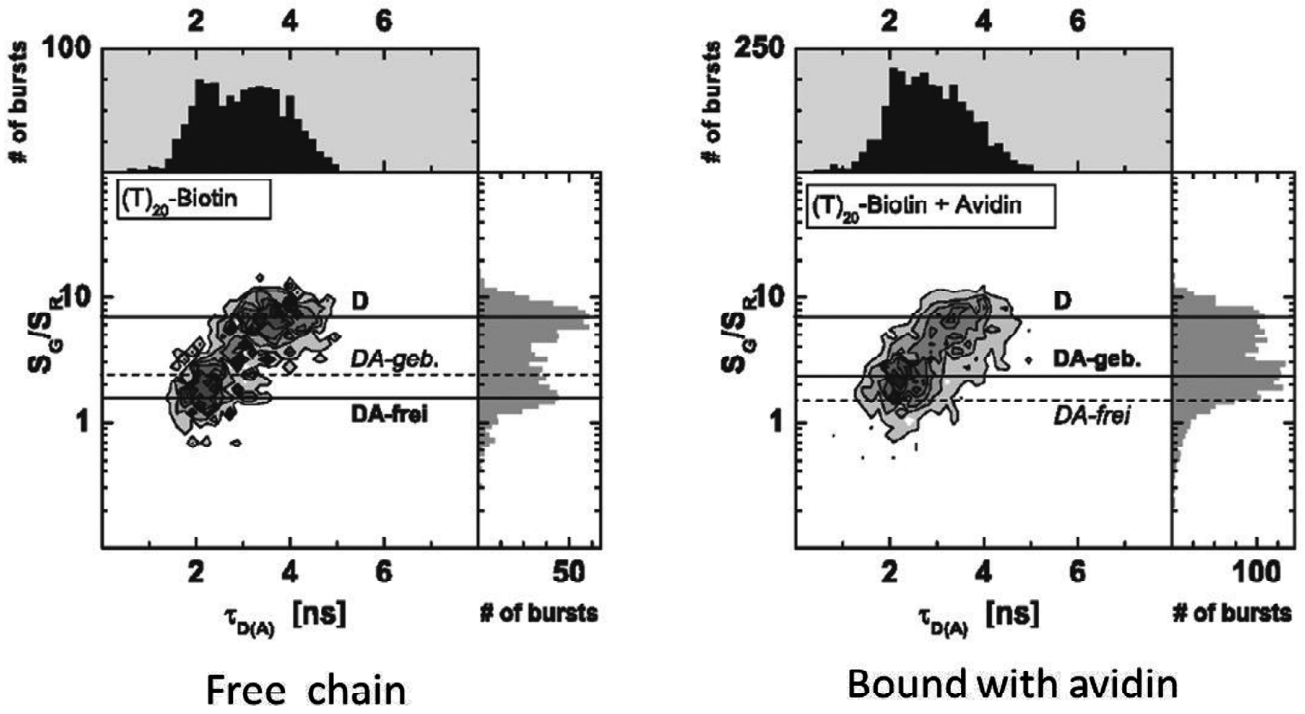

Figure 16: Distributions of S_G/S_R Measured in the Experiment. It is Clearly Seen that S_G/S_R is Larger in the Case of Binding of Avidin

REFERENCES

[1] Hoffmann D., and Moske M., (2003), European Patent EP1363124 24.12.2003. Verfahren Zum Nachweis Eines Analyts Mit Einem Elasto-Optischen Biosensor.

[2] Blagoi G., Rosenzweig N., and Rosenzweig Z., (2005), Design, Synthesis, and Application of Particle-Based Fluorescence Resonance Energy Transfer Sensors for Carbohydrates and Glycoproteins, *Anal. Chem.*, **77**(2), 393-399.

[3] Fan C., Plaxco K. W., and Heeger A. J., (2005), Biosensors Based on Binding-modulated Donor-Acceptor Distances, *Trends. Biotechnol.*, **23**(4), 186-192.

[4] Grosberg A. Y., and Khokhlov A. R., (1994), Statistical Physics of Macromolecules, *AIP Series in Polymers and Complex Materials*, American Institute of Physics.

[5] Español P., (1995), Hydrodynamics for Dissipative Particle Dynamics, *Phys. Rev.*, **E 52**, 1734-1742.

[6] Español P., and Warren P., (1995), Statistical Mechanics of Dissipative Particle Dynamics, *Europhys. Lett.*, **30**(4), 191-196.

[7] Flekkøy E. G., and Coveney P. V., (1999), From Molecular Dynamics to Dissipative Particle Dynamics, *Phys. Rev. Lett.*, **83**, 1775.

[8] Flekkøy E. G., Coveney P. V., and Fabritiis G. D., (2000), Foundations of Dissipative Particle Dynamics, *Phys. Rev.*, **E 62**, 2140-2157.

[9] Vattulainen I., Karttunen M., Besold G., and Polson J. M., (2002), Integration Schemes for Dissipative Particle Dynamics Simulations: From Softly Interacting Systems Towards Hybrid Models, *J. Chem. Phys.*, **116**, 3967-3979.

[10] Hoogerbrugge P. J., and Koelman J. M. V. A., (1992), Simulating Microscopic Hydrodynamic Phenomena with Dissipative Particle Dynamics, *Europhys. Lett.*, **19**, 155-160.

[11] Marx D., (2005), Modellierung und Simulierung Eines Biosensors, Diplomarbeit, Technische Universität München, Zentrum Mathematik, Mathematische Modellierung.

[12] Hoffmann K.-H., Botkin N. D., and Marx D., (2007), Drag on Spheres in Micropolar Fluids with Nonzero Boundary Conditions for Microrotations, *J. Fluid Mech.*, **590**, 319-330.

[13] COSY: Centre of Excellence in Computational Complex Systems Research, Homepage *http://www.lce.hut.fi*

[14] Hinterdorfer P., *et al.*, (2000), Static und Dynamical Properties of Single Poly (Ethylene Glycol) Molecules Investigated by Force Spectroscopy, *Single Molecules*, **1**(2), 123-128.